Journal of Sol-Gel Science and Technology (2019) 90:198–208
https://doi.org/10.1007/s10971-018-4824-6

ORIGINAL PAPER: SOL-GEL AND HYBRID MATERIALS FOR BIOLOGICAL AND HEALTH (MEDICAL) APPLICATIONS

Control of degradation rate of Mg alloys using silica sol–gel coatings for biodegradable implant materials

Yolanda Castro[1] · Alicia Durán[1]

Received: 12 June 2018 / Accepted: 17 September 2018 / Published online: 27 September 2018

Abstract

Silica sol–gel coatings were deposited on AZ31B and AZ91D magnesium substrates with the aim of controlling the degradation rate, corrosion attack and further dissolution of magnesium alloys for temporal implants. Two different silica sols were prepared with and without colloidal silica particles (MTL and TG sols) and deposited by dip-coating on both alloys. The coatings were characterised in SBF using three different in vitro tests; hydrogen evolution, pH variation and potentiodynamic polarization curves. The results show that the corrosion behaviour depends on the alloy and on the coating composition. Coatings on AZ91D-MTL were able to block the degradation of the alloy during 8 days of immersion in SBF, whereas coatings AZ91D-TG only maintain their stability during 3 days. $Mg(OH)_2$ and hydroxyapatite (HAp) were identified as the compounds precipitated on AZ31B samples, not appearing on AZ91D samples. The electrochemical tests confirm the promising corrosion results obtained for coated AZ91D samples.

Graphical Abstract

Suitable silica sol–gel coatings were deposited on Mg alloys showing a great potential to control the degradation rate, corrosion attack and further dissolution of the magnesium alloys.

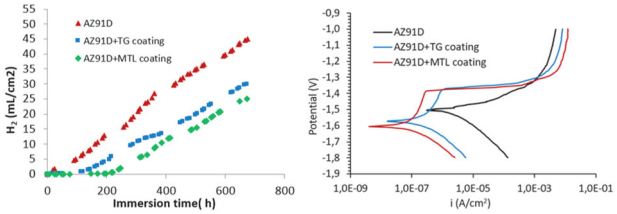

Highlights

- Silica sol–gel coatings are able to block the degradation and corrosion attack of Mg alloys.
- Different corrosion processes were identified that depend on the alloy and composition of the coatings.
- $Mg(OH)_2$ and HAp precipitate onto the alloys, promoting the osteointegration.

Keywords Sol–gel coatings · Mg alloys · Biodegradable

1 Introduction

Metallic materials such as stainless or titanium alloys are widely used as permanent and temporal implants due to their properties such as good mechanical strength and fracture toughness [1–4]. However, they have some important limitations associated with the difference between their elastic moduli with that of natural bone tissue, and also

✉ Yolanda Castro
castro@icv.csic.es

[1] Instituto de Cerámica y Vidrio (CSIC), Campus de Cantoblanco, 28049 Madrid, Spain

with the release of toxic metallic ions and/or particles through corrosion or wear processes [5]. Usually and after repairing, the temporal implants need to be removed by a second surgical procedure [6, 7]. In search of other solutions, magnesium alloys appear as good alternatives for biodegradable implants; the material is gradually corroded during the growth and healing of tissue, being completely dissolved upon fulfilling the regeneration [8].

Mg alloys present several properties similar to natural bone, with density of 1.74-2.0 g/cm^2 compared to 1.8–2.1 g/cm^2 (natural bone), an adequate cyto-compatibility and biocompatibility confirmed through cell culture studies and successful implants in animal models [9, 10]. AZ91D and AZ31B alloys are the more studied alloys for biodegradable purposes. One of the main limitations of magnesium, that currently hinders medical application, is the high corrosion rate, which can influence the survival of living tissues. H_2 is released during the corrosion process affecting the integrity of the implant and avoiding the regeneration of the living materials. On the other hand, the increment of local pH towards alkaline values can induce the poisoning of the cells if pH exceeds 7.8. To solve these limitations is a challenge to open the use of Mg alloys in biomedical applications.

Different ways can be considered to control the corrosion resistance, the most suitable being the surface modification of the alloys by deposition of different films [11, 12]. In this case, the coating should delay the initiation of the corrosion process Mg, further reducing the corrosion rate when it has started. The aim is to maintain the integrity of the substrate for the period needed for ensuring that the implant has fulfilled its restorative function; afterwards, it should degrade up to total dissolution.

Different coating processes have been considered such as galvanic anodization, microarc oxidation (MAO), electrophoretic deposition (EPD), pulsed laser deposition (PLD), etc. [13, 14]. Sol–gel is one of the most widely used methods for anti-corrosive and biocompatible coatings on Mg alloys for orthopaedic applications due to its suitable compatibility with the environment and body [15]. Furthermore, the coatings could be outfitted with other functionalities, such as insertion of drug delivery or precursors for increasing the biocompatibility and bioactivity, etc.

Several strategies have been considered to improve the bioactivity and corrosion resistance of Mg alloys using sol–gel coatings. One important is based in the deposition of bioactive glass or glass–ceramic sol–gel coatings such as Bioglass 45S57, 58S, etc. [16-19]. These materials react with the physiological fluid for obtaining an adequate interfacial bonding with bone by forming a hydroxyapatite layer (HA). Amaravathy et al. [20]. showed, by cell experiments, the biocompatibility and good cell adhesion on HA/TiO_2 sol–gel coatings deposited on Mg alloys confirming the osseointegration. Yang et al. [21] reported the decrease of i_{corr} in more than two orders of magnitude for Mg alloys coated with HA, demonstrating the improvement of in vitro corrosion, and observing an increment in the cyto-compatibility properties. The electrochemical results of bioactive glass–ceramic coatings show a significant control of the corrosion resistance of Mg alloys; initially, degradation proceeds slowly with good cell adhesion and growth, followed by an acceleration [22-24]. Furthermore, the local pH values showed an important decrease, essential to osteoblast cell adhesion and proliferation [23]. For example, 58S MBG coatings immersed in SBF maintain a pH lower than 8 for long immersion time [21, 25].

However, most of these papers report the densification of the coatings at relatively high temperatures (400–450 °C). Mg alloys and specially those of AZ series are very sensitive to temperature [26–28]. In particular, treatment temperatures higher than 200 °C lead to the degradation of the microstructure of AZ91 alloy, affecting the mechanical properties, especially those related to creep [29]. Similar behaviour occurs in AZ31B magnesium alloys. The thermal stability of these alloys can be increased up to 300–350 °C with suitable doping of the alloys [30, 31]; these temperatures being considered as absolute maximum treatment temperature to maintain the mechanical stability of the alloys. Heat treatments overcoming these limits can affect the mechanical stability of the substrate and its behaviour in service.

Another strategy to enhance the corrosion resistance of Mg alloys is the use of inorganic or hybrid sol–gel coatings [32–36]. In this case, most papers report the densification of the coatings at temperatures lower or around 300 °C, to preserve the mechanical properties of the substrate. Nevertheless, these sol–gel coatings are usually designed to obtain suitable barriers for improving the corrosion resistance during long periods of time, not considering their possible use as biodegradable implants [37, 38]. Thereby, the corrosion properties of the metal/coating systems are studied using electrochemical tests in NaCl aqueous solutions, not the simulated body fluid (SBF) [39, 40]. For example, Galio et al. [41]. reported the addition of 8-Hydroxyquinoline (8-HQ) as corrosion inhibitor, into silica-zirconia sol–gel films. The film enhances the corrosion behaviour of the magnesium alloy without degradation of the barrier properties.

Summarizing, only a few papers present a wide-ranging characterization combining electrochemical measurements in SBF with studies of pH and H_2 evolutions, essential properties for application of Mg alloys as biodegradable implant materials [42]. Amaravathy et al. [43] reported a broad characterization of Nb_2O_5 sol–gel coatings on AZ31 alloy for biodegradable implants, including cell adhesion

studies, and informing of a significant reduction of the corrosion rate with formation of HAp after immersion in SBF. However, the coatings were densified at 380 °C/1 h, likely inducing a slight degradation of the mechanical properties of Mg alloy. Gaur et al. [44] studied the in vitro biodegradable properties of silica coatings prepared varying the ratio of silane mixtures. The electrochemical characterization showed an improvement in the corrosion resistance of the coated substrate and a significant decrease in H_2 evolution in SBF. However, the study shows a control of the corrosion degradation for implants that involves short-term but not for long-term protection.

The aim of this work was to develop biodegradable implants using AZ31 and AZ91 standard Mg alloys as substrates, modifying their surfaces through the deposition of inorganic–organic silica sol–gel coatings heat-treated at low temperature (180 °C) to avoid the degradation of the mechanical properties of the alloy. Silica based coating have been selected since they present the best properties on corrosion resistance and biocompatibility. Two different sols were studied, with and without colloidal silica nanoparticles, characterising the mechanical stability, adhesion to the substrate, corrosion resistance as well as the in vitro behaviour of the resulting coatings. The best protective and biocompatible results were obtained for coatings with colloidal silica particles deposited on AZ91D alloy.

2 Experimental

2.1 Substrate preparation

Magnesium alloys AZ31B (Al 3 wt%, Zn 1 wt%, Mn 0.2 wt %, the remaining, Mg) from Dugopa S.A., (Spain) and AZ91D (Al 9 wt%, Zn 1 wt%, Mn 0.33 wt%, Ni 0.002 wt%, Fe 0.005 wt%, the remaining, Mg) from Shaanxi (China) were used as substrates. Before deposition, the alloy sheets were polished with 1200 and 2500 grit SiC paper, followed by ultrasonic cleaning in distilled water.

2.2 Hybrid sol–gel synthesis and characterisation

Two kinds of hybrid silica sols were prepared. First, a hybrid silica sol (TG sol) was synthetized by mixing tetraethoxysilane (TEOS, Aldrich, 99%) and 3-(glycidyloxypropyl)trimethoxy silane (GPTMS, ABCR, 98%) with ethanol absolute (EtOH, Panreac, 99.8%). The solution was stirred for 30 min, after which water acidulated (1N HCl, VWR, 37%) was added to catalyse the hydrolysis and condensation reactions. The final molar ratio of the hybrid silica sol was $TEOS/GPTMS/EtOH/H_2O = 0.5/0.5/3.8/3.5$ and the pH of the sol was 6.

The second hybrid silica sol (MTL sol) was prepared by mixing TEOS and MTES (methyltrietoxysilane, ABCR, 97%) with a colloidal SiO_2 nanoparticles suspension (Ludox-4S, Aldrich, aqueous suspension 40 wt%, particle size 20 nm, pH 9). The solution was stirred for 30 min, after which 0.6 mL of concentrated nitric acid HNO_3 (VWR, 65%) was added to 100 mL of solution. Finally, absolute ethanol was added to the solution to give a final silica concentration of 120 g/L, with 64 g/L of colloidal particles. The final molar ratio of the hybrid silica sol (denoted as MTL) was $TEOS/MTES/SiO_2 = 0.4/0.46/0.14$.

2.3 Deposition and curing of the coatings

The sols were deposited on glass-slides and standard AZ31B and AZ91D substrates (supplied by Dugopa S.A., Spain and Shaanxi, China, respectively) by dip-coating at a withdrawal rate of 30 cm/min and further cured for 30 min at 180 °C. The temperature was selected to prevent the degradation of the mechanical properties of the alloys and to compare both SiO_2 coatings in similar conditions.

2.4 Characterization of the coatings

The coating thickness was measured on coated glass-slides by Spectroscopic Ellipsometer (J.A. Woollam Co., Inc, EC-400, M-2000U Software: WVASE32). The spectral band was recorded from 250 to 900 nm at incident angles between 50° and 60°. The data were fitted using the WVASE32 software with a Cauchy model. Optical microscope (Axiophot-ZEISS, software; ZEN 2012) was utilised to analyse the homogeneity of the coatings and the possible presence of defects, with the help of camera system (AxioCam MRc5).

The morphology and cross-section of coatings deposited on magnesium substrates were studied by scanning electron microscopy (SEM). The adhesion of the coatings was qualitatively measured following ISO 2409 and ASTM D3359 tests. In the test, a pattern of cuts was made in the coating and then a tape is applied and removed over the cuts performed in the film.

In vitro biodegradation studies were developed following three different tests: hydrogen evolution, pH variation and potentiodynamic polarization.

Hydrogen evolution measurements are useful to study the rate of hydrogen evolved and the dissolution rate of magnesium. Uncoated and coated samples of 4 cm^2 were placed in a beaker containing 140 mL SBF solution at 37 °C for 28 days. The hydrogen evolution was evaluated placing a funnel over the sample and a burette vertically mounted over the funnel, then, the dispositive is immersed in the beaker with the SBF (Fig. 1). Experiments were performed

Fig. 1 Photography of dispositive for hydrogen evolution test

Table 1 Composition of simulated body fluid (m-SBF)/liter

Reagents	Amount
NaCl (g)	8.035
$NaHCO_3$ (g)	0.355
Tris [=$(CH_2OH)_3CNH_2$] (g)	6.118
KCl (g)	0.225
$K_2HPO_4{\cdot}3H_2O$ (g)	0.231
$MgCl_2{\cdot}6H_2O$ (g)	0.311
$CaCl_2$ (g)	0.292
Na_2SO_4 (g)	0.072
1 M HCl (ml)	44

in triplicate to evaluate the reproducibility of the test. Table 1 summarizes the composition of SBF.

The pH evolution was measured placing the uncoated and coated samples in a beaker with 140 mL of SBF solution at 37 °C, and monitoring the value as a function of time of immersion up to 14 days. Similar to H_2 evolution, the test was repeated three times to confirm the reproducibility.

The hydrophilic/hydrophobic behaviour of the uncoated and coated substrates was determined by measuring the water contact angle, using the Easy Drop Standard "Drop Shape Analysis System" Kruss DSA 100 equipment under ambient laboratory conditions. Three measurements were performed on each sample and the results are presented as average ± standard deviation.

Fourier transform infrared spectroscopy (FTIR) spectra were recorded between 650 and 4000 cm^{-1}, using a Perkin Elmer Spectrum 100 spectrometer with an attenuated total reflectance (ATR) accessory, with a resolution of 2 cm^{-1}. UV-vis-NIR spectra were recorded between 2500 and 2000 nm with a Perkin Elmer (Lambda 950) spectrophotometer, with a resolution of 2 nm. All spectra were normalized and presented as absorbance (%).

X-ray diffraction (XRD) patterns were obtained with an incident angle of 5° and step size of 0.02° to analyse the presence of hydroxyapatite (HAp).

The corrosion behaviour was studied through potentiodynamic tests performed in SBF solution at 37 °C using a three-electrode system. The uncoated and coated samples (exposed area of 0.78 cm^2) act as working electrode, with platinum as counter electrode and a saturated calomel electrode (SCE) as reference electrode. Open circuit potential was monitored for 12 h and tests were carried out from −1.8 mV/SCE to −1.00 mV at a scan rate of 1 mV/s using a GAMRY Instruments Reference 600 potentiostat. The values of E_{corr} and i_{corr} were determined by Tafel extrapolation method from the potentiodynamic polarization plots. Tests were performed in triplicate.

3 Results and discussion

Both hybrid silica sols (TG and MTL sols) are completely transparent and homogeneous. The addition of silica nanoparticles does not affect the homogeneity of the sol, producing only a slight decrease in the stability with aging time.

The morphology of silica coatings deposited on AZ31B and AZ91D were analysed by optical microscopy to detect lack of homogeneity or defects. The images of optical microscopy showed that the coatings cover perfectly the substrates without detection of cracks, even after curing. The coatings are highly transparent in the visible region; therefore, the optical appearance is not altered. The coating thickness was around 1.5 and 2.5 µm for TG and MTL coatings, respectively.

Figure 2 shows the images of coatings after the tape test. The AZ91D coatings present good adhesion and high mechanical stability, allowing the manipulation of the implant during the surgery. AZ31B coatings show a slight delamination in some part of the cut pattern, that could affect the corrosion behaviour. Analysis of the coating by SEM (not shown) confirmed the good adhesion of the films even after cutting the sample.

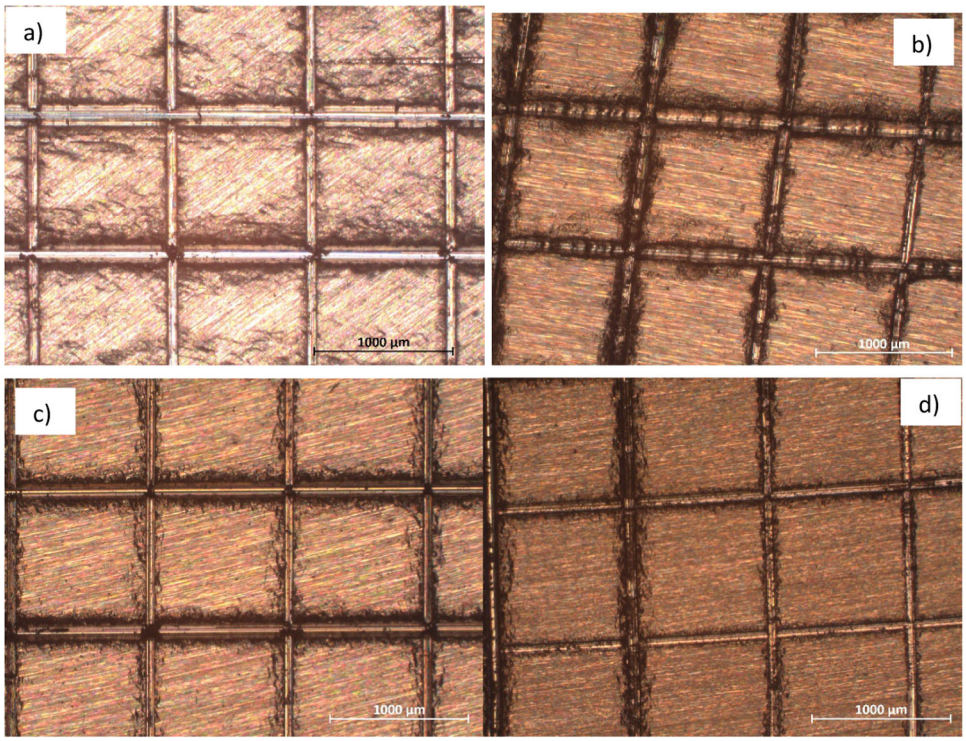

Fig. 2 Appearance of **a** AZ31B-TG, **b** AZ31B-MTL, **c** AZ91D-TG and AZ91D-MTL coatings after applying the adhesion tests

Table 2 Degradation rates and contact angles of uncoated and coated samples

Samples	Degradation rate (mL/cm^2/day)	Contact angle (°)
AZ31B	1.37	85
AZ91D	1.63	70
AZ31B + TG coating	0.163/1.57	72
AZ31B + MTL coating	0.153/1.34	97
AZ91D + TG coating	0.177/1.27	102
AZ91D + MTL coating	0.019/1.31	99

The biodegradation properties of the coatings were followed through the evolution of pH and H_2 as a function of immersion time in SBF. Usually, when Mg alloys is in contact with the physiological environment, corrosion appears. Magnesium hydroxide ($Mg(OH)_2$) and hydrogen gas (H_2) are produced:

$$Mg + 2H_2O \rightarrow Mg(OH)_2 + H_2 \quad (1)$$

with the subsequent local increase of the pH that may affect the cell viability. Initially, $Mg(OH)_2$ could provide a temporary protection of the Mg alloys, retarding the corrosion process, but it is not enough to control the degradation rate (Table 2).

Figure 3 compares the hydrogen evolution for the alloys AZ31B and AZ91D uncoated and coated with TG and MTL sols during 28 days of immersion in SBF solution.

In a first step, the hydrogen evolution on bare alloys is different respecting to coated ones. In the case of AZ31B a typical parabolic law is observed [40], probably associated with a diffusion-controlled process that can be explained considering the precipitation of insoluble and protective magnesium hydroxide or corrosion products on the surface. The images of AZ31B uncoated samples as a function of immersion time (Fig. 4) support this hypothesis. Instead, the corrosion of AZ91D is close to a linear tendency, different to the parabolic law for the AZ31B. The mechanism of corrosion changes, probably related with the different alloying elements present in AZ91D compared to AZ31B. The degradation rate, determined considering a lineal degradation process, was 1.37 and 1.63 mL/cm^2/day, for AZ31B and AZ91D alloys, respectively, although the real degradation rate for a parabolic behaviour should be greater (Table 3).

Figure 4 shows the different morphology and corrosion process depending of the alloy. In AZ31B, white corrosion products ($Mg(OH)_2$) are observed on the surface; otherwise

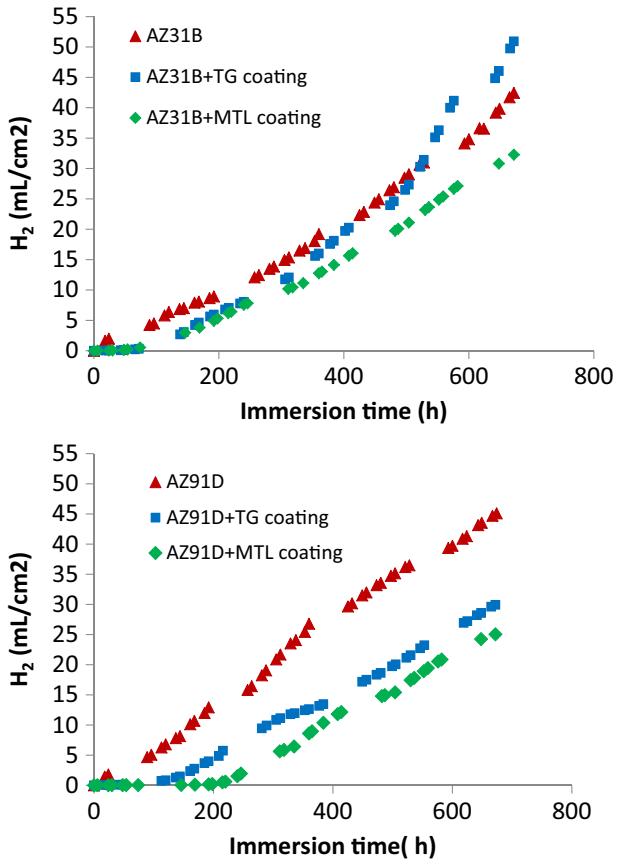

Fig. 3 Variation of hydrogen evolution as a function of immersion time in SBF solution for coated and uncoated **a** AZ31B and **b** AZ91D substrates

on AZ91D practically not corrosion products appear. The amount of corrosion products increases with the immersion time, especially on the AZ31B.

In the case of coated samples, the hydrogen evolution with the immersion time shows a different behaviour compared to bare substrates, depending on the alloy and type of silica coating. It is clearly observed that coated AZ91D samples suffer less corrosion respecting to coated AZ31B. For AZ91D-MTL film, the hydrogen evolution is very slow during the first 200 h (8 days) of immersion, less than 0.5 mL/cm^2. For AZ91D-TG coating, there is a control only for the first 120 h (5 days). Other authors have reported the diminution of the H_2 evolution for coated AZ91D samples but not so marked. For example, Chen et al. [45] reported low H_2 values of 0.5 mL/cm^2 but only during the first 100 h of immersion.

During this first period, the degradation rate (Table 3) was determined obtaining values of 0.019 and 0.177 mL/cm^2/day, respectively. Silica coatings, especially MTL,

Table 3 Electrochemical parameters obtained from potentiodynamic polarization curves

Sample	E_{corr}	i_{corr}(μA/cm^2)
AZ31B	−1.44	6.23
AZ91D	−1.50	1.75
AZ31B + TG coating	−1.51	0.15
AZ31B + MTL coating	−1.60	0.3
AZ91D + TG coating	−1.57	0.14
AZ91D + MTL coating	−1.58	0.04

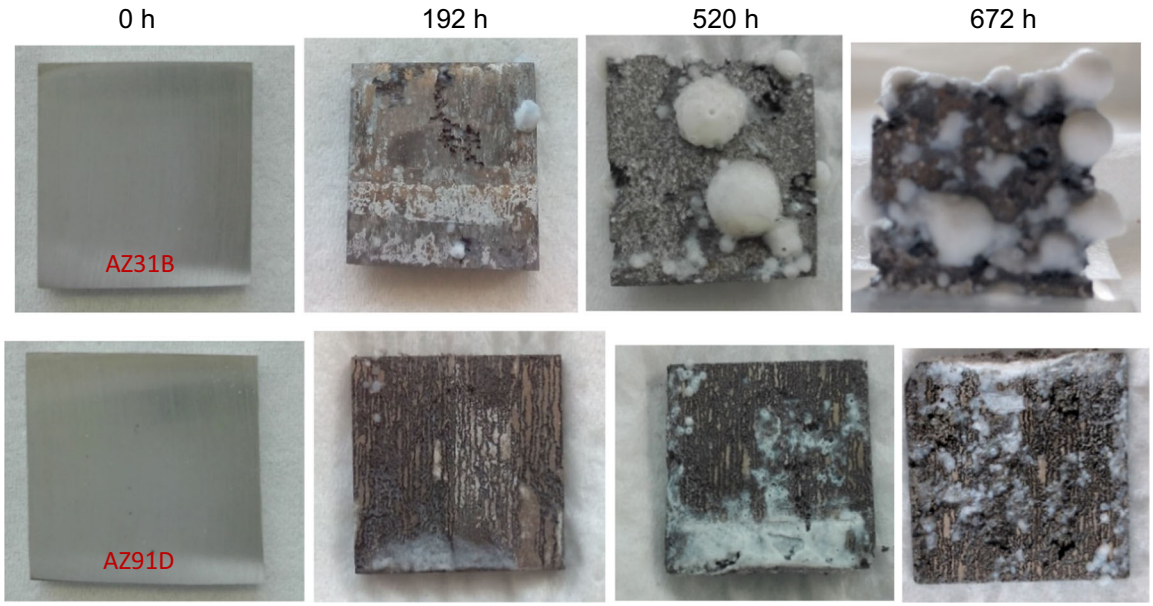

Fig. 4 Optical images of **a** AZ31B and **b** AZ91D substrates after immersion in SBF for 672 h

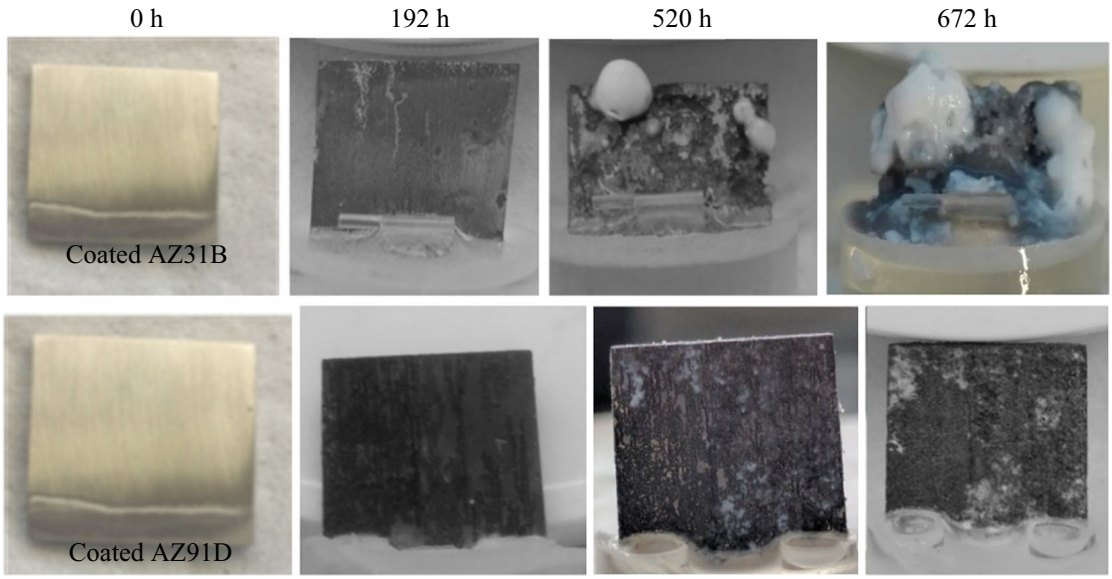

Fig. 5 Optical images of coated **a** AZ31B and **b** AZ91D substrates after immersion in SBF for 672 h

were able to control the degradation rate of the magnesium, blocking the corrosion during the first days of immersion in SBF. Afterwards, the degradation starts, reaching values of 1.27 and 1.31 mL/cm^2/day, very similar in both cases. For coated AZ31B and during the first 70 h, the corrosion process is slower (0.6 mL/cm^2) respecting to the bare alloy and similar for both silica films. The coatings offer only temporary protection to the substrate. Values of 0.163 and 0.153 mL/cm^2/day were determined for AZ31B-TG and AZ31B-MTL, respectively. After this time, AZ31B-TG coating degradation accelerates (1.57 mL/cm^2/day) respecting to AZ31B-MTL coating (1.34 mL/cm^2/day), even surpassing the bared alloy (1.37 mL/cm^2/day). The difference between both alloys and with the information reported by other authors could be associated with the different adhesion properties observed in the adhesion tests (Fig. 2).

Figure 5 shows the images of AZ31B-TG and AZ91D-TG coatings with the immersion time up to 672 h (28 days). AZ31B-TG shows a higher degradation along with the deposition of $Mg(OH)_2$ and HAp. On the other hand, AZ91D-TG samples suffer lower degradation but the precipitation of corrosion products was not appreciated, probably associated with the conversion of $Mg(OH)_2$ into soluble $MgCl_2$ [43].

Summarising, AZ91D-MTL coating appears as the most adequate to control the degradation rate of the alloy, although the stability of the corrosion products is worse, and the possibility to grow HAp on the implant is lower, which could affect the generation of the tissue.

Surface wettability plays an important effect in the corrosion behaviour. Table 3 shows the measurements of uncoated and coated substrates when a drop of SBF was placed on the surfaces. For uncoated samples, AZ91D substrate has the lowest contact angle, about 70°, implicating higher surface energy and more hydrophilic behaviour compared to AZ31B (85°). After the deposition of silica coatings, the contact angle greatly increases reaching a maximum value around 100° for AZ31B-MTL, AZ91D-TG and AZ91D-MTL coatings. Thus, the coated surfaces are more hydrophobic than the bare substrate and the penetration of SBF could be reduced, enhancing the corrosion resistance of the coated system, as observed in the hydrogen degradation plots. The contact angle decreases from 85 up to 72° for AZ31B-TG coating, explaining the rapid degradation of the substrate when the corrosion starts. Hydrophobic surfaces may be not suitable, because the cell adhesion can be affected. In the future, supplementary tests will be performed to study the cell adhesion on bare and coated samples.

FTIR spectra obtained from coated samples before and after the test of hydrogen evolution are shown in Fig. 6. The spectra of AZ91D-MTL samples before and after the test are very similar. The principal bands associated with the of Si–O–Si bonds, ~940–1200 cm^{-1}, are identified, indicating that the silica coating is still present after 28 days of immersion. This behaviour explains the better corrosion resistance of AZ91D-MTL sample respecting to coated AZ31B and uncoated specimens. On the other side, for AZ31B-MTL sample the silica coating has completely disappeared after the test. Only bands associated to $Mg(OH)_2$, at 1375 cm^{-1} attributed to O–H vibration of $Mg(OH)_2$ together with bands associated with carbonate groups (1380 cm^{-1}) and phosphate PO_4^{3-} (560–1110 cm^{-1}) groups of

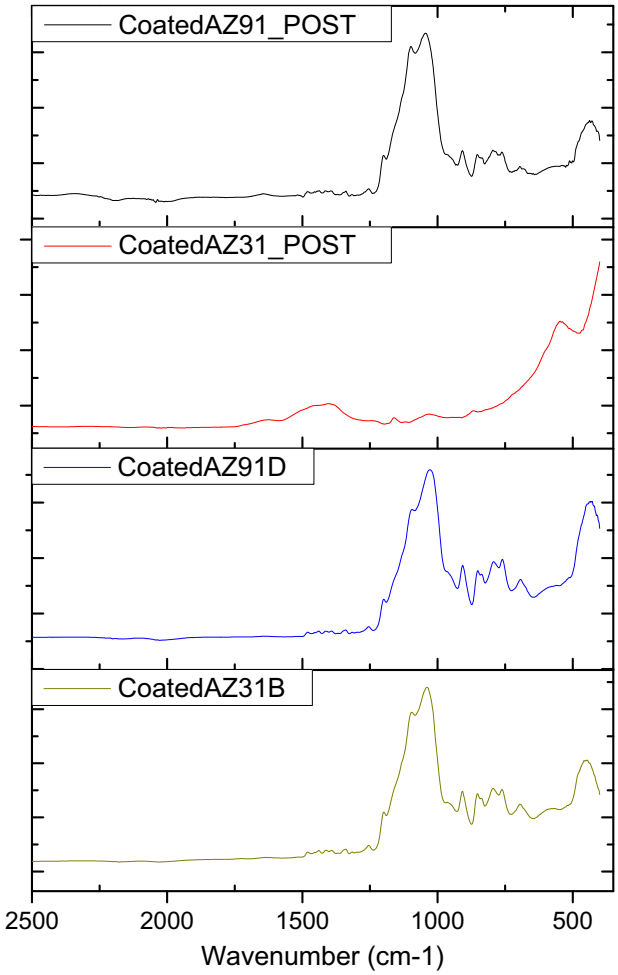

Fig. 6 FTIR spectra obtained from coated samples before and after the test

HAp appear [46]. For coated AZ91D, it is not possible to identify the bands due to overlapping and poor adhesion of the corrosion products in the surface (Fig. 4). The corrosion products layer, mainly constituted by magnesium hydroxide, magnesium phosphate and calcium magnesium phosphate, are not stable, providing only a temporary protection [20].

XDR diffraction of the AZ31B-MTL coating was performed after 28 days of immersion (Fig. 7). The absence of peaks associated with amorphous SiO_2, around 20°, indicates that the silica coating has disappeared at the end of test confirming the results obtained by FTIR (Fig. 6c). Peaks associated with $Mg(OH)_2$ and HAp are identified according to the JCPDS-00-009-432 and 00-044-1482 data, respectively. In the case of coated AZ91D samples, the poor adhesion of the corrosion products avoids the identification of $Mg(OH)_2$ and HAp by XRD.

The evolution of the pH with the time in SBF solution has been also analysed, Fig. 8, showing a tendency similar to that observed on the hydrogen evolution curves. In the

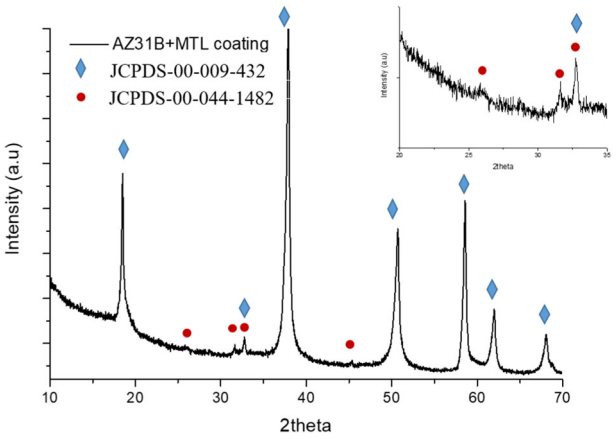

Fig. 7 XRD spectrum of the top surface of AZ31B-TG coating after 28 days of immersion in SBF

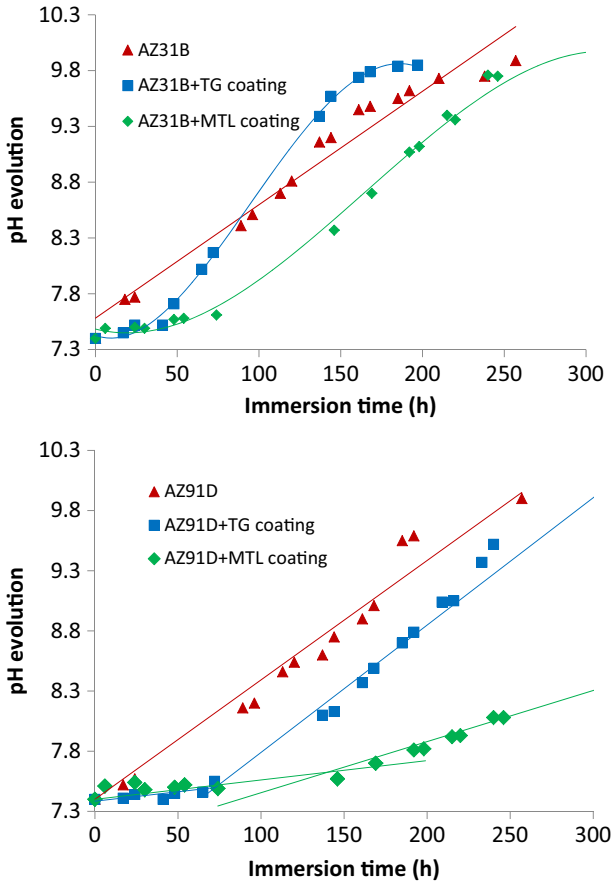

Fig. 8 Variation of pH as a function of immersion time in SBF solution for coated and uncoated **a** AZ31B and **b** AZ91D substrates

case of AZ31B, the pH increases after 24 h of immersion in SBF. The deposition of a silica coating delays the biodegradation process during the first 2 days; as time prolongs, the increment is very rapid, not suitable for the human body. For AZ91D-MTL coating the pH maintains below 7.5 for

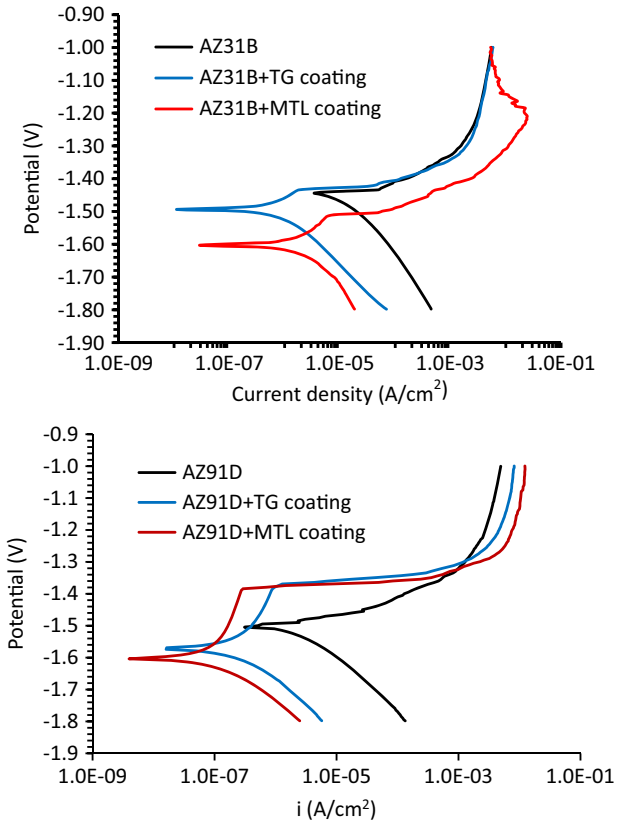

Fig. 9 Potentiodynamic polarization curves of **a** the magnesium AZ31B with and without coatings; **b** the magnesium AZ91D with and without coatings

more than 6 days compared to uncoated and coated AZ91D-TG sample. The stability of the coating is markedly higher for AZ91D-MTL coating compared to the rest of the coatings and alloys. The pH is a critical factor to ensure a good bone regeneration and the formation of HAp.

Figure 9 shows the potentiodynamic polarization figures for the bare and coated samples in SBF at 37 °C. The corrosion potential (E_{corr}) and the corrosion current density (i_{corr}) have been estimated and the values are summarized in Table 3. The corrosion potential slightly changes between coated and uncoated samples. Similar behaviour was observed for 58S sol–gel coatings on AZ31B and AZ91D alloys [16]. However, all the coated samples show much lower i_{corr} compared to the naked alloys, indicating an increasing of the corrosion resistance. The maximum improvement was observed for AZ91D-MTL coating, with a i_{corr} of 4×10^{-8} A/cm^2 compared to 1.75×10^{-6} A/cm^2 for bare alloy, two orders of magnitude lower. A similar effect was observed for hydrogen evolution. Some authors [36, 47] have reported the electrochemical characterization of sol–gel coatings on AZ91D, observing a change in the E_{corr} to more positive values and a drop in the i_{corr} ($\sim 1 \times 10^{-7}$ A/cm^2) respect to bare substrate, finding that the sol–gel layers could provide a good corrosion protection. However, the values of i_{corr} determined were higher than that observed to AZ91D-MTL coating, resulting the coating with the best corrosion resistance properties. On the other hand, AZ91D-TG, AZ31B-TG and AZ31B-MTL films show similar values of corrosion current density, around $\sim 1 \times 10^{-7}$ A/cm^2, close to those reported.

For all coated samples, the anodic part shows a passivation range indicating the existence of a protective film on the surface. This passive region depends on the coating composition, being much higher for AZ91D coated samples respecting to ones. A breakdown potential of −1.38 V is observed for both AZ91D samples compared to −1.43 V and −1.5 V, corresponding to AZ31B-TG and AZ31B-MTL films, respectively. Thus, silica coatings on AZ91D alloy provide a more effective physical barrier against corrosion. On the other hand, the anodic part of potentiodynamic curves for uncoated samples show no passivation region, with high corrosion rates from the initial time. These results, including the amplitude of passivation regions, are similar or better than the published results [44, 47, 48].

To sum up, the corrosion resistance of AZ91D magnesium alloy was significantly improved with the deposition of silica coatings, confirming and reinforcing the results of hydrogen evolution and pH tests for this alloy. The coatings inhibit the diffusion of active corrosion ions and water, showing much lower degradation rates. The coated AZ91D could thus be used to control the degradation rate of Mg for future biodegradable implant. TG and MTL coatings may be useful for fitting the degradation process more suitable depending on the application.

The aim is to maintain slow degradation rates up to the finishing of the restoring process (stents, bone healing, etc.) with the further acceleration of the dissolution of the alloy after this process.

Further work is in progress to introduce bioactive glass particles for promoting the deposition of HAp on the AZ91D alloy and EIS tests for following the evolution of corrosion with time.

4 Conclusions

In summary, reproducible and environmentally friendly silica sol–gel coatings were deposited on AZ31B and AZ91D substrates showing a great potential to control the degradation rate and corrosion attack of magnesium alloys.

Both electrochemical (potentiodynamic) and non-electrochemical (H_2 and pH evolution) tests were used to evaluate the corrosion behaviour of silica coatings on magnesium alloys. Different corrosion processes appeared depending on the alloy and composition of the coatings. In general, coated AZ91D samples reduce more significantly the H_2 release and decrease pH values compared to coated

AZ31B samples. On the other hand, the MTL coating can block the degradation of magnesium during more prolonged time, 8 days, than TG coatings, only 3 days. However, the stability of corrosion products and HAp deposition is worse in AZ91D substrate.

The electrochemical corrosion tests show a relevant effect on the protection of magnesium alloys by the deposition of silica films. This improvement is more important in MTL coating for AZ91D substrates.

The results obtained in this work reveal that it is possible to select the suitable alloy and coating composition, depending on the application of the implant, to reach the required anti-corrosion properties and the further dissolution of Mg substrates after the specific reparation is finished.

Acknowledgements This work was supported by MINECO under Projects MAT2017-87035-C2-1-P/2-P (AEI/FEDER, UE). The authors would like to thank to Aritz Iglesias and Irene Ramirez Ruiz for their helpful in the develop of the experimental part.

Compliance with ethical standards

Conflict of interest The authors declare that they have no conflict of interest.

References

1. Mantripragada VP, Lecka-Czernik B, Ebraheim NA, Jayasuriya AC (2013) An overview of recent advances in designing orthopedic and craniofacial implants. J Biomed Mater Res A 101:3349–3364. https://doi.org/10.1002/jbm.a.34605
2. García C, Ceré S, Durán A (2004) Bioactive coatings prepared by sol-gel on stainless steel 316L. J Non Cryst Solids 348:218–224. https://doi.org/10.1016/j.jnoncrysol.2004.08.172
3. Ballarre J, López DA, Rosero NC et al. (2008) Electrochemical evaluation of multilayer silica-metacrylate hybrid sol-gel coatings containing bioactive particles on surgical grade stainless steel. Surf Coat Technol 203:80–86. https://doi.org/10.1016/j.surfcoat.2008.08.005
4. Kulkarni M, Mazare A, Gongadze E et al. (2015) Titanium nanostructures for biomedical applications. Nanotechnology 26. https://doi.org/10.1088/0957-4484/26/6/062002
5. Cramers M, Lucht U (1977) Metal sensitivity in patients treated for tibial fractures with plates of stainless steel. Acta Orthop 48:245–249. https://doi.org/10.3109/17453677708988763
6. Zheng YF, Gu NX, Witte F (2014) Biodegradable metals. Mater Sci Eng R 77:1–34. https://doi.org/10.1007/978-1-4614-3942-4_5
7. Wolford ML, Palso K, Bercovitz A (2015) Hospitalization for total hip replacement among inpatients aged 45 and over: United States, 2000–2010. NCHS Data Brief, No. 186
8. Fischer J, Prosenc MH, Wolff M et al. (2010) Interference of magnesium corrosion with tetrazolium-based cytotoxicity assays. Acta Biomater 6:1813–1823. https://doi.org/10.1016/j.actbio.2009.10.020
9. Agarwal S, Curtin J, Duffy B, Jaiswal S (2016) Biodegradable magnesium alloys for orthopaedic applications: a review on corrosion, biocompatibility and surface modifications. Mater Sci Eng C 68:948–963. https://doi.org/10.1016/j.msec.2016.06.020
10. Ding Y, Lin J, Wen C et al. (2016) Mechanical properties, in vitro corrosion and biocompatibility of newly developed biodegradable Mg-Zr-Sr-Ho alloys for biomedical applications. Sci Rep 6:1–10. https://doi.org/10.1038/srep31990
11. Hornberger H, Virtanen S, Boccaccini AR (2012) Biomedical coatings on magnesium alloys - a review. Acta Biomater 8:2442–2455. https://doi.org/10.1016/j.actbio.2012.04.012
12. Goodman SB, Yao Z, Keeney M, Yang F (2013) The future of biologic coatings for orthopaedic implants. Biomaterials 34:3174–3183. https://doi.org/10.1016/j.biomaterials.2013.01.074
13. Gray JE, Luan B (2002) Protective coatings on magnesium and its alloys — a critical review. J Alloy Compd 336:88–113. https://doi.org/10.1016/S0925-8388(01)01899-0
14. Narayanan TSS, Park I-S, Lee M-H (2015) Surface modification of magnesium and its alloys for biomedical applications. Elsevier Ltd, Woodhead Publishing, Singapore
15. Owens GJ, Singh RK, Foroutan F et al. (2016) Sol-gel based materials for biomedical applications. Prog Mater Sci 77:1–79. https://doi.org/10.1016/j.pmatsci.2015.12.001
16. Omar S, Castro Y, Ballarre J et al. (2017) Magnesium alloys implants coated with 58S sol gel bioactive glass to retard first stage corrosion. Corrosion 9312:2508. https://doi.org/10.5006/2508
17. Shen S, Cai S, Xu G et al. (2015) Influence of heat treatment on bond strength and corrosion resistance of sol–gel derived bioglass–ceramic coatings on magnesium alloy. J Mech Behav Biomed Mater 45:166–174. https://doi.org/10.1016/j.jmbbm.2015.02.005
18. Wang X, Cai S, Xu G et al. (2013) Surface characteristics and corrosion resistance of sol–gel derived $CaO–P_2O_5–SrO–Na_2O$ bioglass–ceramic coated Mg alloy by different heat-treatment temperatures. J Sol-Gel Sci Technol 67:629–638. https://doi.org/10.1007/s10971-013-3122-6
19. Dou Y, Cai S, Ye X et al. (2013) 45S5 bioactive glass–ceramic coated AZ31 magnesium alloy with improved corrosion resistance. Surf Coat Technol 228:154–161. https://doi.org/10.1016/j.surfcoat.2013.04.022
20. Amaravathy P, Sathyanarayanan S, Sowndarya S, Rajendran N (2014) Bioactive HA/TiO_2 coating on magnesium alloy for biomedical applications. Ceram Int 40:6617–6630. https://doi.org/10.1016/j.ceramint.2013.11.119
21. Yang H, Yan X, Ling M et al. (2015) In vitro corrosion and cytocompatibility properties of nano-whisker hydroxyapatite coating on magnesium alloy for bone tissue engineering applications. Int J Mol Sci 16:6113–6123. https://doi.org/10.3390/ijms16036113
22. Ye X, Cai S, Dou Y et al. (2012) Bioactive glass–ceramic coating for enhancing the in vitro corrosion resistance of biodegradable Mg alloy. Appl Surf Sci 259:799–805. https://doi.org/10.1016/j.apsusc.2012.07.127
23. Huang K, Cai S, Xu G et al. (2014) Sol-gel derived mesoporous 58S bioactive glass coatings on AZ31 magnesium alloy and in vitro degradation behavior. Surf Coat Technol 240:137–144. https://doi.org/10.1016/j.surfcoat.2013.12.026
24. Huang K, Cai S, Xu G et al. (2013) Preparation and characterization of mesoporous 45S5 bioactive glass–ceramic coatings on magnesium alloy for corrosion protection. J Alloy Compd 580:290–297. https://doi.org/10.1016/j.jallcom.2013.05.103
25. Ren M, Cai S, Liu T et al. (2014) Calcium phosphate glass/MgF2 double layered composite coating for improving the corrosion resistance of magnesium alloy. J Alloy Compd 591:34–40. https://doi.org/10.1016/j.jallcom.2013.12.215
26. Wang F, Hu T, Zhang Y et al. (2017) Effects of Al and Zn contents on the microstructure and mechanical properties of Mg-Al-Zn-Ca magnesium alloys. Mater Sci Eng A 704:57–65. https://doi.org/10.1016/j.msea.2017.07.060

27. Cheng-wen T, Xu S, Wang L et al. (2007) Effect of temperature on mechanical behavior of AZ31 magnesium alloy. Trans Nonferrous Met Soc China 17:41–45. https://doi.org/10.1016/S1003-6326(07)60045-4
28. Ren M, Cai S, Xu G et al. (2013) Influence of heat treatment on crystallization and corrosion behavior of calcium phosphate glass coated AZ31 magnesium alloy by sol–gel method. J Non Cryst Solids 369:69–75. https://doi.org/10.1016/j.jnoncrysol.2013.03.022
29. Čížek L, Greger M (2006) Mechanical properties of magnesium alloy AZ91 at elevated temperatures. Achiev 18:203–206
30. Mahmudi R, Kabirian F, Nematollahi Z (2011) Microstructural stability and high-temperature mechanical properties of AZ91 and AZ91 + 2RE magnesium alloys. Mater Des 32:2583–2589. https://doi.org/10.1016/j.matdes.2011.01.040
31. Cardinal S, Malchère A, Garnier V, Fantozzi G (2009) Microstructure and mechanical properties of TiC-TiN based cermets for tools application. Int J Refract Met Hard Mater 27:521–527. https://doi.org/10.1016/j.ijrmhm.2008.10.006
32. Reyes Y, Durán A, Castro Y (2016) Glass-like cerium sol-gel coatings on AZ31B magnesium alloy for controlling the biodegradation of temporary implants. Surf Coatings Technol 307. https://doi.org/10.1016/j.surfcoat.2016.09.056
33. Córdoba LC, Montemor MF, Coradin T (2016) Silane/TiO_2 coating to control the corrosion rate of magnesium alloys in simulated body fluid. Corros Sci 104:152–161. https://doi.org/10.1016/j.corsci.2015.12.006
34. Singh IB, Gupta P, Maheshwari A, agrawal N (2015) Corrosion resistance of sol – gel alumina coated Mg metal in 3. 5 % NaCl solution. J Sol-Gel Scie Technol 73:127–132. https://doi.org/10.1007/s10971-014-3503-5
35. Li Q, Zhong X, Hu J, Kang W (2008) Preparation and corrosion resistance studies of zirconia coating on fluorinated AZ91D magnesium alloy. Prog Org Coatings 63:222–227. https://doi.org/10.1016/j.porgcoat.2008.06.004
36. Hu J, Li Q, Zhong X, Kang W (2008) Novel anti-corrosion silicon dioxide coating prepared by sol–gel method for AZ91D magnesium alloy. Prog Org Coatings 63:13–17. https://doi.org/10.1016/j.porgcoat.2008.03.003
37. Lamaka SV, Montemor MF, Galio AF et al. (2008) Novel hybrid sol–gel coatings for corrosion protection of AZ31B magnesium alloy. Electrochim Acta 53:4773–4783. https://doi.org/10.1016/j.electacta.2008.02.015
38. Luo F, Li Q, Zhong XK et al. (2012) Corrosion electrochemical behaviors of silane coating coated magnesium alloy in NaCl solution containing cerium nitrate. Mater Corros 63:148–154. https://doi.org/10.1002/maco.201005706
39. Zhong X, Li Q, Hu J et al. (2010) A novel approach to heal the sol–gel coating system on magnesium alloy for corrosion protection. Electrochim Acta 55:2424–2429. https://doi.org/10.1016/j.electacta.2009.11.063
40. El-Hadad AA, Barranco V, Samaniego A et al. (2014) Influence of substrate composition on corrosion protection of sol–gel thin films on magnesium alloys in 0.6M NaCl aqueous solution. Prog Org. Coatings 77:1642–1652. https://doi.org/10.1016/j.porgcoat.2014.05.026
41. Galio AF, Lamaka SV, Zheludkevich ML et al. (2010) Inhibitor-doped sol–gel coatings for corrosion protection of magnesium alloy AZ31. Surf Coat Technol 204:1479–1486. https://doi.org/10.1016/j.surfcoat.2009.09.067
42. Majumder O, Singh Bankoti AK, Kaur T et al. (2016) The influence of silane and silane–PMMA coatings on the in vitro biodegradation behavior of AE42 magnesium alloy for cardiovascular stent applications. RSC Adv 6:107344–107354. https://doi.org/10.1039/C6RA23384H
43. Amaravathy P, Sowndarya S, Sathyanarayanan S, Rajendran N (2014) Novel sol gel coating of Nb2O5 on magnesium alloy for biomedical applications. Surf Coat Technol 244:131–141. https://doi.org/10.1016/j.surfcoat.2014.01.050
44. Gaur S, Singh Raman RK, Khanna AS (2014) In vitro investigation of biodegradable polymeric coating for corrosion resistance of Mg-6Zn-Ca alloy in simulated body fluid. Mater Sci Eng C Mater Biol Appl 42:91–101. https://doi.org/10.1016/j.msec.2014.05.035
45. Chen B, Li Q, Gao H et al. (2009) Microstructural characteristics and corrosion property of non-chromate surface treatments on AZ91D magnesium alloy. Mater Corros 60:521–526. https://doi.org/10.1002/maco.200805167
46. Baji A, Wong S-C, Liu T, Li TSS T (2007) Morphological and X-ray diffraction studies of crystalline hydroxyapatite-reinforced polycaprolactone. J Biomed Mater Res B Appl Biomater 83:340–344. https://doi.org/10.1002/jbmb
47. Zhong X, Li Q, Chen B et al. (2009) Effect of sintering temperature on corrosion properties of sol-gel based Al_2O_3 coatings on pre-treated AZ91D magnesium alloy. Corros Sci 51:2950–2958. https://doi.org/10.1016/j.corsci.2009.08.031
48. Zaharescu M, Predoana L, Barau A et al. (2009) SiO_2 based hybrid inorganic–organic films doped with TiO_2–CeO_2 nanoparticles for corrosion protection of AA2024 and Mg-AZ31B alloys. Corros Sci 51:1998–2005. https://doi.org/10.1016/j.corsci.2009.05.022